Periodic bunches produced by electron beam squeezed states in a resonant cavity

Cite as: Phys. Plasmas **27**, 083103 (2020); https://doi.org/10.1063/5.0014620
Submitted: 20 May 2020 . Accepted: 16 July 2020 . Published Online: 04 August 2020

M. Siman-Tov, J. G. Leopold, Y. P. Bliokh, and Ya. E. Krasik

Physics of Plasmas ARTICLE scitation.org/journal/php

Periodic bunches produced by electron beam squeezed states in a resonant cavity

Cite as: Phys. Plasmas **27**, 083103 (2020); doi: 10.1063/5.0014620
Submitted: 20 May 2020 · Accepted: 16 July 2020 ·
Published Online: 4 August 2020 · Publisher error corrected: 6 August 2020

M. Siman-Tov,[a] J. G. Leopold, Y. P. Bliokh, and Ya. E. Krasik

AFFILIATIONS

Physics Department, Technion-Israel Institute of Technology, Haifa 320003, Israel

[a]Author to whom correspondence should be addressed: meytalsh2@gmail.com

ABSTRACT

We have carried out experiments with a squeezed state of a magnetized high current electron beam, which produces a high-frequency, ∼200 MHz periodic train of tens of amperes electron bunches. The results of particle in cell simulations confirm the formation of a squeezed state and electron bunch generation. However, the frequency of modulation in simulations was ∼1 GHz. The reasons for this discrepancy are discussed.

I. INTRODUCTION

The limiting current of a strongly magnetized high-current annular electron beam, propagating in a uniform conducting tube, depends on the energy of electrons and the ratio of the tube, R, to beam r_b radii. For a thin mono-energetic annular beam in a tube much longer than its radius, the limiting current, that is, the maximum current supporting steady flow, is given by[1,2]

$$I_{LC} = 17\left(\gamma^{2/3} - 1\right)^{3/2}/[2\ln(R/r_b)](\mathrm{kA}), \tag{1}$$

where γ is the relativistic factor. To evaluate this equation, Brejzman and Ryutov[1] assumed that the electrostatic potential is the same everywhere along the beam. They also found that the functional characterizing it has two solutions. If more I_{LC} is injected, the system does not necessarily stabilize at the limiting current. Then, the system may stabilize near one of the two solutions. One, when the beam velocity is high and its density (charge/unit length) becomes low; and the second, when the beam velocity becomes slow and its density is high. The latter was named by Ignatov and Tarakanov a *squeezed state*,[3] who realized such a state in simulations of a tube with a higher radius downstream section. A detailed theoretical analysis appears in Refs. 4 and 5, and squeezed states were experimentally realized by Belomyttsev *et al.*[6] When the tube is non-uniform, i.e., a combination of cylindrical sections with different radii, the determined current is limited by that in the highest radius section. If the largest radius section is placed downstream and the current produced upstream exceeds the limiting current of this section, part of the electrons is reflected back near the position of the tube radius transition (RT) point. The rest of the electrons continue their motion downstream, so that the beam near the RT forms a virtual cathode (VC). Since this VC is detached from the emitter, this VC is an *extended* VC.[3] For a pictorial demonstration of squeezed states and extended VCs, see Refs. 3 and 7. The upstream (reflected) current, when it reaches the cathode, reduces the emitted current so that the downstream current becomes less than the limiting current of the downstream section. This stops the VC formation near the RT and reduces the upstream current so that, in turn, it increases emission from the cathode and restores the VC, and so on periodically. To obtain Eq. (1), Brejzman and Ryutov[1] assumed that the current source and the beam's downstream end are at infinite distances. For this case, the system's reaction to over-injection, that is, either higher electron velocity and lower beam density or lower electron velocity and higher beam density, did not necessitate such two stream flows. In the presence of a RT, a return electron flow develops in an attempt to reduce the emitted current. In the region between the emitter and the RT, the second solution of the original single stream problem becomes stable, that is, lower energy higher charge, a squeezed state. Such systems were studied in many publications because dense low energy electron plasmas found applications in microwave producing devices.[8,9]

Our interest was to force the extended VC to oscillate rather than to relax a squeezed state. We proposed to use three consecutive tube sections of radii $r_2 < r_1 < r_3$ instead of three sections of increasing radius $r_1 < r_2 < r_3$, often used to produce squeezed states.[7] Because the limiting current is highest in the mid-section of the proposed choice, the extended VC's oscillations prevail over squeezing producing electron bunches which may be used in accelerators or microwave

devices. A second slowing down voltage reflector in the third section was also added in simulations, which increases the upstream current and, consequently, the charge density in the extended VC causing more distinct beam oscillations.[7] Here, let us note another method of electron bunches formation, based on high-frequency (up to 10 MHz) modulation of the cathode electron emission, studied numerically in Ref. 10.

To add, a second slowing down high voltage source (>100 kV) is an experimental difficulty. In the present paper, we propose a simple method to slow down the beam using only a single source. We found though that for this configuration, a squeezed state forms, but the additional energy reduction is insufficient for the current leakage of the squeezed state to oscillate. On the other hand, this current leakage excites an electromagnetic eigenmode of an adjacent cavity which modulates the beam and a periodic train of electron bunches is produced. This interaction is very similar to that observed in transit time oscillators (monotrons).[11–13]

In this paper, we present the results of an experiment and numerical simulations of the periodic modulation of a squeezed electron beam. There is a difference between the modulation frequencies, obtained in the MAGIC particle-in-cell (PIC) simulations[14] and that observed experimentally. The reason for this discrepancy is discussed.

II. PIC SIMULATIONS

We consider a setup with the cylindrically symmetric geometry seen in Fig. 1. A coaxial cathode–anode system produces an annular electron beam emitted from the edge (emitter) of a cathode. The anode has a single RT at a certain distance, $d_{e\text{-}t}$, from the emitter. The entire system is immersed in a uniform axial magnetic field of 1 T.

We add a *reflector* which is a conducting circular thin grid attached to the cathode at its center by a conducting central rod and placed inside a ring, which reduces the electric field enhancement at the grid's edge. The reflector grid is considered to be completely transparent to electrons, and scattering from the grid is neglected. The amplitude of the electron current emitted from the cathode exceeds that of the limiting current in the larger diameter tube section. This causes the formation of the VC near the RT. The current is partially reflected from the VC toward the emitter and when the reflected

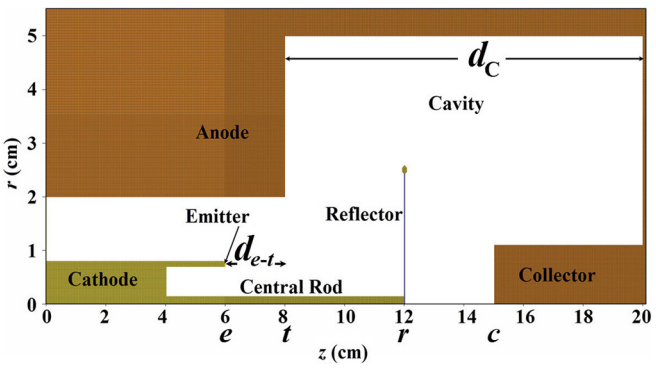

FIG. 1. The cylindrical symmetrical geometry of the PIC simulated system. *e*, *t*, *r*, and *c* point out the position of the emitter edge, RT, reflector, and collector, respectively.

electron charge reaches the emitter, the emitted current decreases. The rest of the beam flows downstream from the VC to the reflector and when the absolute value of the potential in front of the reflector becomes larger than that of the reflector, a part of the beam will be ejected toward the collector. The collector is attached to the anode tube by an end flange placed at a certain distance, d_C, from the RT. In the experiment, this collector is a low-inductance and low-resistance Faraday cup which measures the current arriving to the collector. Otherwise, it can be a tube through which the beam advances further.

A voltage of ∼150 kV rising in 20 ns is applied between the cathode and the grounded anode. The calculated limiting currents[1,2] for a cathode radius of 8 mm and anode radii of 2 and 5 cm (see Fig. 1) are 750 and 380 A, respectively. First, we consider the system in Fig. 1 without the central rod, reflector, and the collector. The electron momentum phase-space $[z, p_z]$ at 35 ns shown in Fig. 2(a) displays the extended VC which has developed between the RT and the emitter and the electron flow to the end flange. Some flow to the upstream boundary is also seen. In Fig. 2(b), we draw the time dependence of the total, emitted, and collected currents. The total current is measured near the upstream end of the system in Fig. 1, and the current is collected on the downstream end flange. In Fig. 2(b), there is a small drop in the total current at ∼11 ns pointed out by an arrow. This is exactly at the time when the electron flow returning from the RT, where the VC is formed, reaches the emitter causing a reduction of the total current. The latter though continues to rise with the rising voltage reaching ∼400 A, close to the predicted limiting current value. From this point, all currents are stable; the total and collected current are almost equal (∼395 A), slightly lower than the emitted current due to small contributions from upstream currents collected on the emitter, the cathode and a small upstream electron current which exits through the open boundary.

Next, we add the central rod and reflector (Fig. 1 without the collector). This system is characterized by a completely different phase space structure [Fig. 2(c)] than that seen in Fig. 2(a). The extended VC is not discerned anymore, and the forward and backward flows reach lower momenta. Also, one can see a larger flow upstream from the emitter. In Fig. 2(d), we draw the same currents as those in Fig. 2(b). The extended VC does develop during the rise time and its formation accompanied by appearance of return current and reduces the emitted current [see arrow pointing at the red curve in Fig. 2(d)], the total current, and even the collected current at about the same times as in Fig. 2(b). Following this point in time, the emitted current increases with the voltage but the total current reduces until it reaches the value of the steady state total current [see arrow at ∼20 ns in Fig. 2(d)]. The steady state emitted current reaches ∼110 A, whereas the total and collected currents reach ∼30 A. We calculated the upstream currents collected on the emitter, the cathode, and the upstream open boundary to be ∼30, 5, and 50 A, respectively, which explains the difference between the emitted current and the total and collected current. Also, this means that in the gap between the emitter and the reflector, there is a downstream flow of ∼110 A and, at the same time, an upstream flow of ∼85 A. The small current fluctuations at $t > 20$ ns in Fig. 2(d) are evidence of some instability of the flow in the emitter—reflector interval. These fluctuations have no distinct frequency. The reduction of the steady state collected current, ∼400 A [Fig. 2(b)], to ∼40 A [Fig. 2(d)] is evidence as to how effectively the reflector returns current toward the emitter.

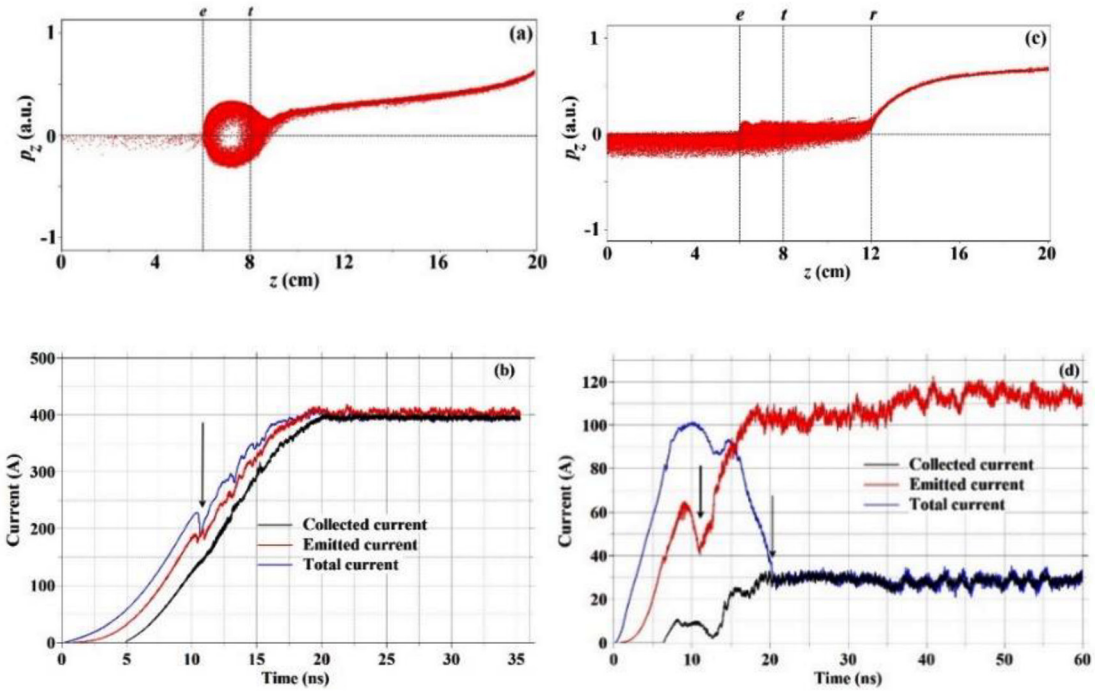

FIG. 2. (a) The [z, p_z] phase space at $t = 35$ ns and (b) the time dependence of the total, emitted, and collected (on the end flange) currents for the geometry of Fig. 1 but without the central rod, reflector, and collector. (c) and (d) are the same as (a) and (b), respectively, but with the rod and reflector included. ***e***, ***t***, and ***r*** point out the position of the emitter, RT, and reflector, respectively.

The effect of the reflector on the longitudinal electron density distribution is seen in Fig. 3(a). Without the reflector, the electron density peaks near the edges of the extended VC at a density higher by a factor of ∼2 compared to the region in between. Within the extended VC the electrons flow down- and up-stream with a maximum average kinetic energy of 40–50 keV while slowing down at both ends [Fig. 3(b)]. When the reflector is present, there is low-energy flow from and toward the reflector and also a flow downstream from it. The latter is due to electron space charge buildup leading to a negative potential larger than the emitter potential in the space between the reflector and the collector.

In the experiment, we intended to add a Faraday cup within the boundaries of the collector seen in Fig. 1. PIC simulations show that the presence of the collector changes drastically the system behavior. This is demonstrated in Fig. 4, where the temporal evolution of the collected current is presented for an applied voltage of 170 kV and a distance of 3 cm between the reflector and the collector. Up to ∼60 ns, the time dependence and current values in Fig. 4 are similar to the

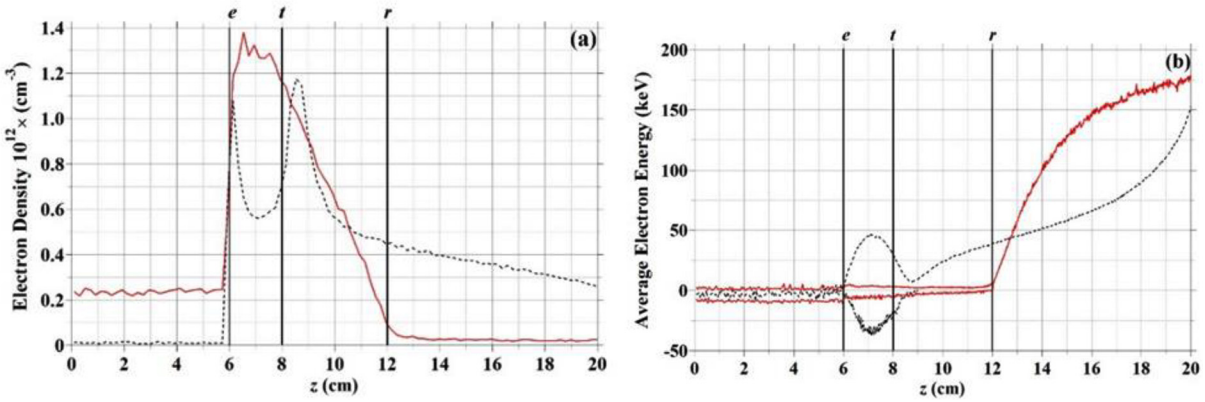

FIG. 3. (a) Electron density measured in $\Delta z = 2$ mm wide axial bins vs z for the cases in Fig. 2(a) (dotted line) and Fig. 2(c) (red solid line). (b) The average energy of electrons flowing downstream (positive values) and of electrons flowing upstream (negative values) for the case in Fig. 2(a) (dotted black lines) and in Fig. 2(c) (red solid lines).

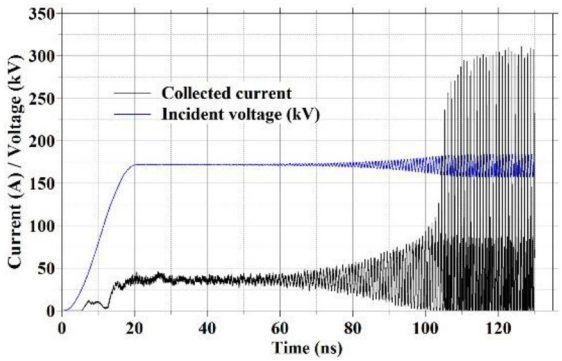

FIG. 4. The voltage at the upstream boundary and the current collected on the collector of Fig. 1 vs time.

case when the collector is absent [Fig. 2(d)]. Then, the current starts to oscillate with increasing amplitude reaching values higher by an order of magnitude. The time dependence of the collected current seen in Fig. 4 is very similar to that observed in monotrons (see Ref. 11), where the oscillatory behavior of the current develops as a result of the interaction between an axial beam and a nearby cavity which is similar to the situation seen in Fig. 1.

In Fig. 5(a), we follow the details of the dynamics in a few cycles of the large current oscillations of Fig. 4. $[z, p_z]$ phase space frames are displayed in Fig. 5(b). There are two detachments of the beam from the collector at times where the current is zero, each followed by current peaks, first the smaller peak and then the larger peak in Fig. 5(a). We shall explain this below. One should note in Fig. 5(b), that the squeezed state between emitter and the reflector acts as the current source to the interval between the reflector and the collector. Also, an almost constant current of ~60 A flows upstream from the emitter. The longitudinal electron density distribution and the average kinetic energy of the electrons at the same time as the phase space frames in Fig. 5(b) are presented in Figs. 5(c) and 5(d), respectively. The electron density (at most $\sim 1.5 \times 10^{12}\,\mathrm{cm}^{-3}$) and average electron energy (a few keV) in the region between the emitter and reflector change little in time.

In order to establish the reasons for this oscillatory behavior, the effect of some geometrical parameters was studied. The current on the collector for various values of the cavity lengths, d_C, while all other dimensions are kept constant, is plotted in Fig. 6.

The main oscillation frequency is 1.13 GHz [Figs. 4 and 5(a)], and higher harmonics are also present in the waveform. We calculated the eigenfrequencies of the downstream cavity including the collector in the absence of the beam for $d_C = 11$, 12, 13, and 14 cm and found these to be 1.35, 1.15, 1.00, and 0.89 GHz, respectively. The most significant frequencies of the large current oscillations in Fig. 6 are 1.13, 1.03, and 0.88 GHz for $d_C = 12$, 13, and 14 cm, respectively, which are close to the calculated eigenfrequencies. However, oscillations were not excited for $d_C = 11$ cm up to the times considered. It is important to note that no oscillations are observed when the Faraday cup is moved further downstream so that the reflector—Faraday cup distance becomes larger than that for the cases discussed here. These peculiarities indicate that the current oscillations develop when certain relations between the electron transit time and the cavity eigenfrequency are satisfied as is the case for monotrons. For the system considered, this relation is difficult to determine because of the complex dynamics of electrons in the squeezed state and in the reflector–collector gap and the complex structures of the cavity eigenmodes.

We have designed an experiment to demonstrate the predictions made in this section, that is, that a squeezed state can interact with a nearby cavity to produce high frequency, high amplitude current oscillations, or else electron bunches. As will be seen below, the experiment produced electron bunches but instead of hundreds of amperes oscillating at ~1 GHz, we obtain ~40 A, 2 ns long electron bunches at a frequency of ~200 MHz. We attempt to explain these results by considering the differences between the experimental system and the one simulated in this section.

III. THE EXPERIMENTAL SETUP

The pulsed power source used in the experiments was a bipolar Marx generator[15] which consists of 12 pulse forming network stages each of ~7 Ω impedance and a pulse duration of ~250 ns. When a matched resistive load of ~84 Ω is attached, the amplitude of the generator's high voltage output pulse was ~140 kV and ~200 kV, for a charging voltage of ±25 kV and ±35 kV, respectively. The high voltage pulse was applied on a 16 mm-diameter cylindrical hollow cathode consisting of 25 carbon capillaries (1 mm/0.5 mm outer/inner diameter, 3 mm long) attached to the circular perimeter of a hollow aluminum cathode holder (see Fig. 7). Earlier studies show that this type of cathode has low threshold voltage (<15 kV/cm) for plasma formation allowing electron beam generation of several kA/cm^2 current density.[16] A 40 mm diameter anode, made from a 2 mm thick aluminum tube, was placed coaxially inside a 122 mm diameter stainless steel tube. The downstream part of this tube is to be considered the larger radius anode section with a radial transition from 20 mm to 60 mm. The cathode was coaxially located inside the anode with its edge placed typically at a distance of 20 mm from the anode's radial transition point. The anode– cathode radial gap was 12 mm adjusted within ±0.1 mm. The reflector was a 100 μm thick Molybdenum foil covered with 1 mm diameter perforated holes so that it had a geometrical transparency of ~28%. The foil was supported by a 40 mm diameter aluminum ring coated with ~100 μm thick alumina (Al_2O_3) ceramic. Earlier research[17] shows that such coating prevents surface explosive plasma formation for electric fields up to ~300 kV/cm. The reflector was connected to the cathode by a 3 mm diameter aluminum central rod (see Fig. 7). The distance between the reflector and the anode radial transition point could be varied between 20 and 40 mm. The inductance of an 80 mm long central rod can be estimated to be ~45 nH which induces a ≤1 kV voltage drop between the cathode and reflector for a current rise time $\leq 2 \times 10^{10}$ A/s, typical to the present experiment.

For the parameters of the present experiment, when the amplitude of the applied high voltage is ≤200 kV, the magnetic field necessary for the efficient operation of the magnetically insulated diode should be $B > 3B_{cr}$, where $B_{cr} = 3.4(\gamma^2 - 1)r_C/(r_A^2 - r_C^2) \approx 0.8$ kG is the critical magnetic field,[18,19] $r_C = 0.8$ cm and $r_A = 2$ cm are the cathode and anode radii, respectively, $\gamma = 1 + e\varphi_C/mc^2 \leq 1.4$ is the relativistic factor; m and e are the charge and mass of the electron,

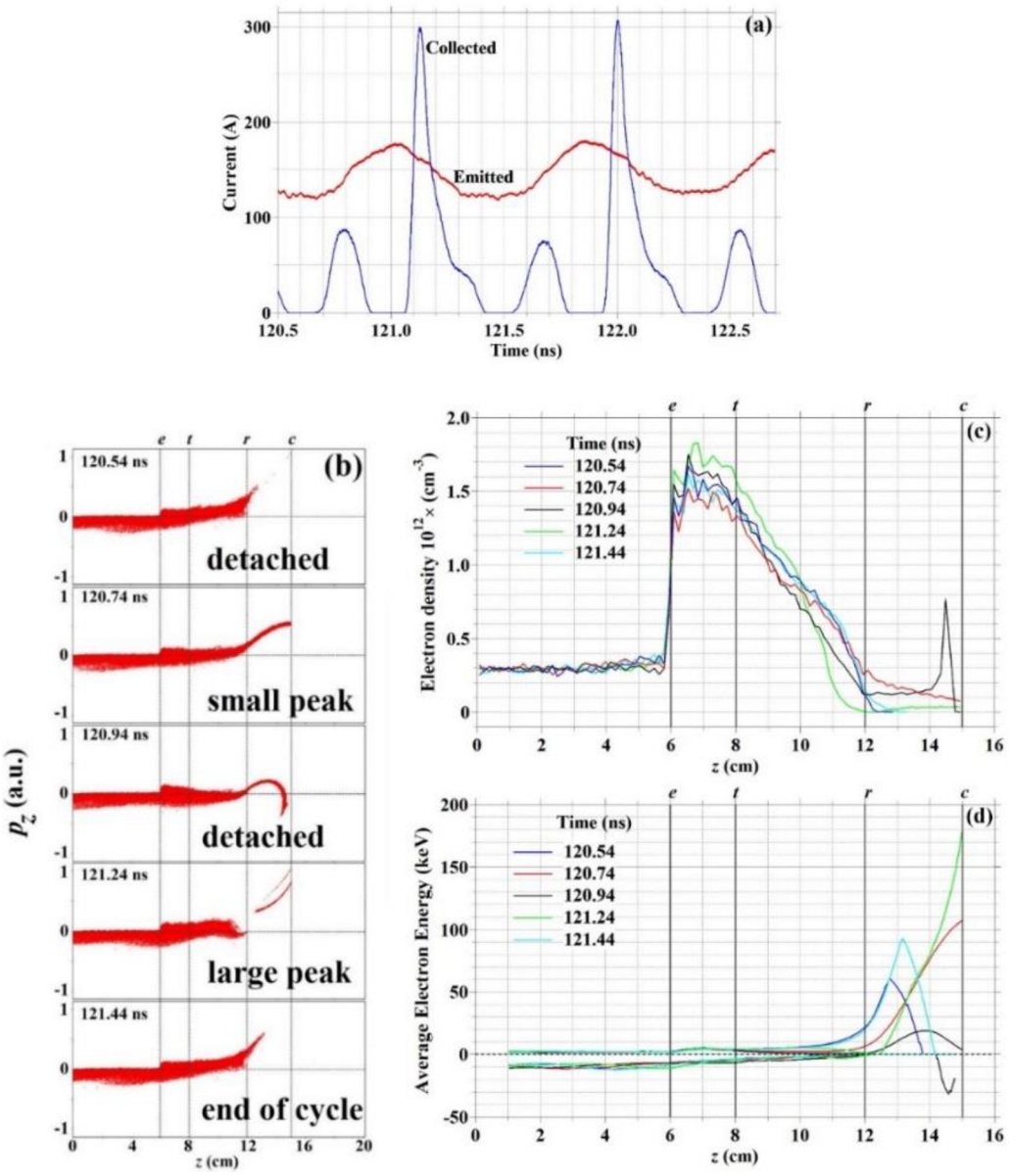

FIG. 5. (a) An enlarged time interval from Fig. 4 with the time dependence of the collected current overlaid with the emitted current. (b) The [z,p_z] momentum phase space at consecutive times within the time interval of (a). The longitudinal electron density distribution (c) and the average electron energy of electrons flowing downstream (positive values) and electrons flowing upstream (negative values) (d), at the times depicted in (b).

respectively; φ_C is the cathode potential; and c is the speed of light. In the experiment, the magnetic field was produced by a solenoid, wound around the stainless steel tube (see Fig. 7) and powered by a 4.1 mF capacitor, preliminarily charged to 1250 V and discharged by a triggered vacuum spark gap. The solenoid produced a 1 T pulsed (15 ms half period) axial magnetic field, sufficiently long so that the skin effect related to the magnetic field diffusion through the stainless steel tube's wall and the anode is negligible. Applying a 1 T magnetic field, one can estimate the thickness of a hollow electron beam[20] as $\delta \approx 1.4 \times E[MV/cm] \times B^{-2}[\mathrm{T}] \approx 0.4\,\mathrm{mm}$, where $E = \varphi_c[\mathrm{MV}]r_c^{-1}[\mathrm{cm}]ln^{-1}(r_A/r_c) = 0.273\,\mathrm{MV/cm}$ is the electric field at the open edge of the carbon capillary for cathode potential $\varphi_c \approx 200\,\mathrm{kV}$. In practice, the thickness of the beam wall can be larger because of electric field enhancement at the capillary edge and the explosive plasma's radial expansion across the magnetic field with a velocity of $\sim 2 \times 10^5$ cm/s,[19,21] which results in $\sim$1 mm during the $\sim$250 ns of the high voltage pulse. Also, let us note that the transverse energy $\varepsilon_\perp = mV_\perp^2/2$, acquired by electrons

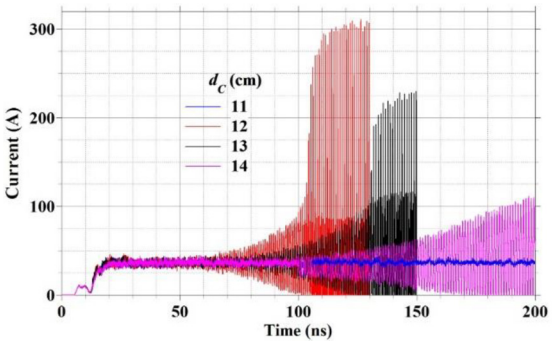

FIG. 6. The current collected on the collector in Fig. 1 for $d_{e\text{-}t} = 2$ cm and various values of d_C.

in the azimuthal drift by the $E_r \times B_z$ fields does not exceed 6. Thus, the value of the limiting current[1,2] of the electron flow in the region where the stainless steel tube radius is $r_t = 60$ mm and the energy of electrons is <200 keV is 420 A, above which a VC should form.

The waveforms of the voltage applied to the diode and the total current were measured using a resistive voltage divider and a self-integrating Rogowski coil, respectively. The electron beam current was measured by a movable Faraday cup consisting from a graphite collector covered by a 70% transparency stainless steel grid and a low-inductance current viewing 0.1 Ω resistor. The distance between the Faraday cup and the reflector was varied in the range 20–80 mm. An additional flange (not shown in Fig.7) of diameter equal to that of the stainless steel external tube with a central circular hole of a diameter equal to the external diameter of the Faraday cup could also be added. Moving this flange along the Faraday cup holder, the length of the larger radius anode section, d_C, could be changed. Two B-dot probes were used to measure the time dependence of the total current flowing in the cathode holder and the electron beam current arriving to the Faraday cup (see Fig. 7). A vacuum level of 10^{-3} Pa was kept in the system by a turbo-molecular and scroll pumps.

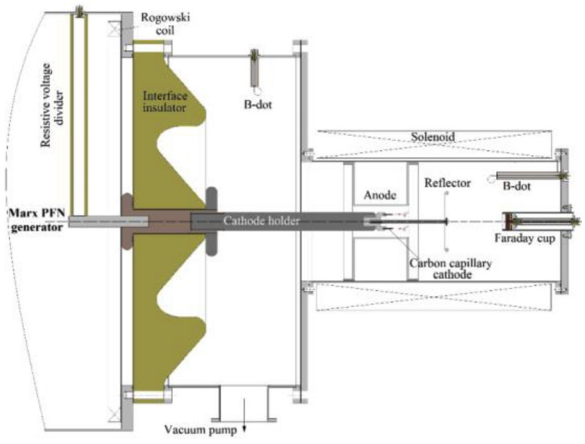

FIG. 7. Experimental setup.

IV. EXPERIMENTAL RESULTS

In the absence of the reflector and central rod, typical waveforms of the voltage, total current, and electron current collected by the Faraday cup when placed at a distance of 75 mm from the anode radial transition point are shown in Fig. 8(a). In Fig. 8(b), the electron beam pattern, obtained at a distance of 75 mm from the anode radial transition point on a CR-39 film, is shown. One can see that the beam pattern has a satisfactory azimuthal uniformity and the width of the pattern suggests a beam energy deposition of ≤2 mm which reflects an azimuthally uniform plasma from the carbon capillaries surface and strong magnetization of the electrons. One can see that electron beam generation begins with a time delay of a few ns relative to the beginning of the voltage applied to the cathode, the result of almost simultaneous plasma formation on the carbon capillary surface. The increase in the amplitude of the voltage pulse is accompanied by increasing current so that at ∼180 kV, the total and electron beam current reach the values ∼900 A and ∼450 A, respectively. The value of the current collected on the Faraday cup is close to that obtained in the simulations in Fig. 2(b). The measured total current is though much higher. This is because the Rogowski coil and the $\dot{B}$ probe (see Fig. 7) are placed in a region where the axial magnetic field is zero while the return electron flow is shunted downstream to the cavity walls. Thus, these probes measure only the current flowing in the cathode holder [see, for example, Fig. 10(a) below]. The difference between the measured total current and the collected current gives the value of the return current emitted from the cathode plasma toward the generator. The collected electron beam current is limited by the limiting current [Eq. (1)] determined by the ratio of the anode segment with the largest radius to the beam radius (∼450 A for our experiment). The oscillations seen on the waveforms of the current and voltage at $t \sim$ 200–300 ns could be the result of partial shorting by the explosive emission plasma formed in the cathode–Faraday cup gap and that at the surface of the Faraday cup grid. These plasmas can propagate toward each other along the magnetic field expanding with velocities of $\sim 2 \times 10^7$ cm/s.[19,21] The voltage and total current oscillations during the current rise time are probably due to non-simultaneous operation of the gas spark switches of the Marx generator.

In Fig. 9(a), we present the experimental results when the reflector is placed between the anode and Faraday cup at a distance of 40 mm from the RT and 30 mm from the Faraday cup. One can see a drastic change in the waveform of the current of the electron beam collected on the Faraday cup. Namely, the current collected on the Faraday cup rises in ∼20 ns and displays deep high-frequency modulations present during the entire voltage pulse to amplitudes reaching ∼40 A. A time delay of ∼10 ns exists between the appearance of the current at the Faraday cup and the appearance of the voltage and total current. FFT [Fig. 9(b)] and time-frequency analysis [Fig. 9(c)] show that the dominant modulation frequency is ∼200 MHz present during the entire pulse and a much weaker high frequency component of ∼1.17 GHz which decays after ∼200 ns is discerned. The modulations are very deep suggesting the existence of a periodic sequence of electron bunches, each of ∼2 ns duration. The voltage pulse shape in Fig. 9(a) has a rise time of ∼50 ns followed by a ∼200 ns long plateau and no oscillations at $t \sim 250$ ns as in Fig. 8(a). This difference can be explained by the predicted lower energy squeezed electrons in the cathode–reflector space which leads to significantly lower plasma density formation on the reflector surface and, consequently no

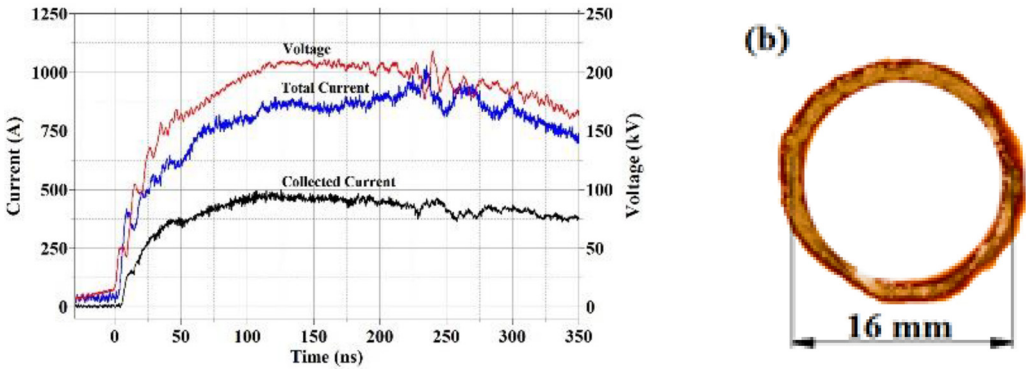

FIG. 8. (a) Waveforms of the voltage, total current, and electron beam current collected on the Faraday cup placed 75 mm from the anode radial transition point. (b) Electron beam pattern obtained on a CR-39 film placed at the same position as the Faraday cup in (a).

reflector-cathode gap shorting. The total current rises together with the voltage to ∼400 A, from where it decreases fast to ∼300 A. After ∼40 ns, it increases again during ∼15 ns to ∼500 A followed by a gradual increase to ∼750 A. These voltage and current waveforms recur in all our experiments and for different values of the applied high voltage pulse amplitudes.

Penetration of the electron beam through the reflector which has almost the same potential as the cathode, starts only when sufficient charge accumulates near the reflector surface forming a VC in front of it at a potential φ_{VC} lower that the cathode potential, φ_C. The ∼10 ns time delay in the appearance of electrons at the Faraday cup is probably the accumulation time of this electron space charge sufficient to make $|\varphi_{VC}| > |\varphi_C|$. This delay can also be observed in the simulations (Fig. 4), but the later simulated time dependence is completely different from the experiment. The first plateau at ∼300 A in the total current can be explained by the steady state reached by the electron space charge in the between the cathode and the reflector leading to quasi-constant space charge limited emission from the cathode. The second gradual increase in the total current close to the total current obtained in the absence of the reflector [Fig. 8(a)] can be explained by the formation of a dilute plasma at the reflector ring surface resulting in electron emission toward the anode downstream flange. Indeed, visual inspection of this flange showed typical patterns caused by the electron flow from the reflector ring. One can estimate that the energy density deposition of ∼150 keV, ∼100 A/cm^2 electrons during ∼40 ns into the stainless steel flange are greater than 100 J/g sufficient for plasma

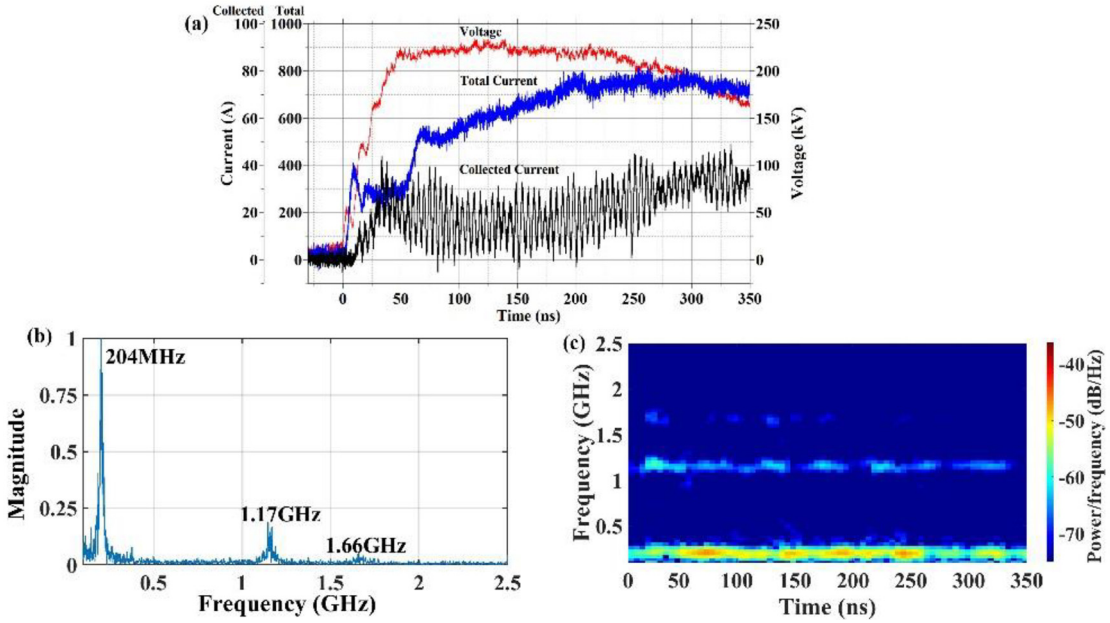

FIG. 9. (a) Typical waveforms of the voltage, total, and collected currents with the reflector placed at the distance of 40 mm from the anode output and 30 mm from the collector; (b) Fast Fourier transform of the collected current; (c) short-time Fourier transform of the collected current.

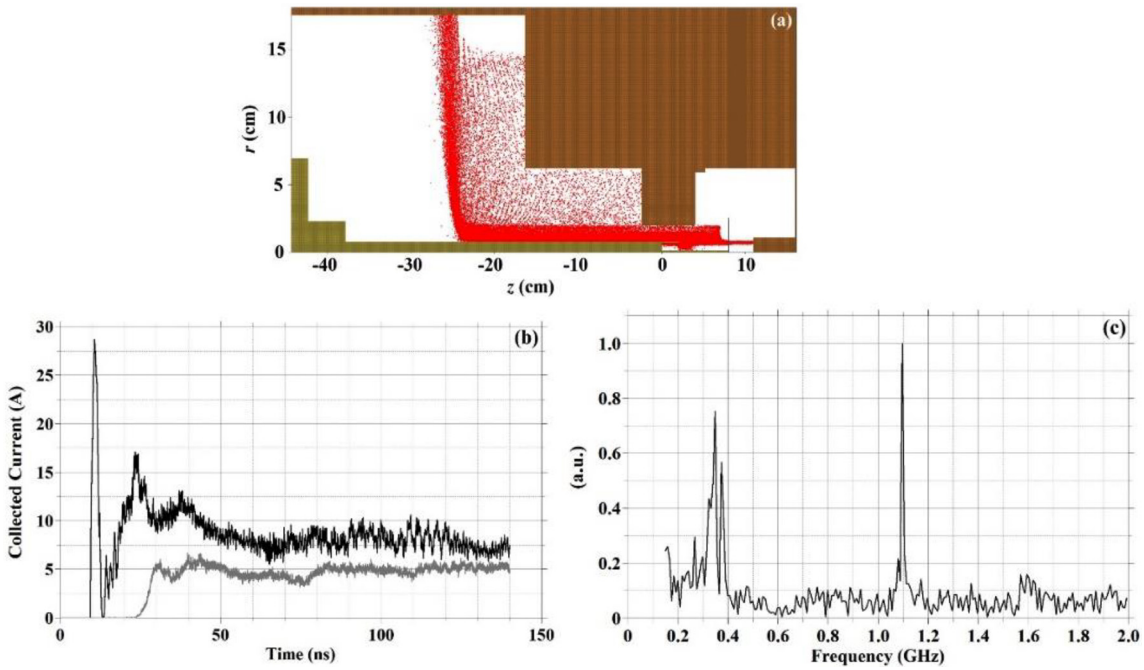

FIG. 10. (a) Electron positions at 140 ns in the system including the upstream section of the experiment. (b) The current collected on the Faraday cup (black) and on the walls of the upstream cavity (gray). (c) Spectrum of the current collected on the Faraday cup in (b).

formation. The plasma, formed at the anode flange surface, can be considered as a source of ion flow toward the reflector thus partially compensating the space charge of the electron beam in this space. Also, the gradual increase in the total current after ∼40 ns can be related to the radial and axial expansion of the cathode plasma.

In an attempt to obtain the predicted large current oscillations related in Sec. II to beam cavity interactions, we performed experiments by varying the distance d_C between the RT and the downstream flange while keeping all other distances fixed. The experimental results were insensitive to the change in the cavity depth with all results similar to those seen in Fig. 9. The results were also insensitive to different RT—reflector distances for fixed reflector—Faraday cup distance or vice versa.

Finally, for different charging voltages of the Marx generator, we checked the effect of the amplitude of the applied high-voltage pulse. We found that increasing the applied voltage leads to the decrease in the duration of the first plateau of the total current [Fig. 9(a)] in qualitative agreement with our explanation related to the plasma formation on the reflector surface. Also, the increase in the amplitude of the voltage from ∼160 to ∼220 kV results in the increase in the total current and the current modulations amplitudes by a factor of ∼1.5, while the frequency of the modulations remains unchanged.

In addition to the plasma formed at the surface of the perforated Mo foil, we think that in the experiment, there were some additional plasma sources form the surface of the Mo-foil ring holder and at the surface of the central bolt used to connect the foil to the central rod. These plasmas served as a source of additional electron flow toward the anode increasing the total current amplitude which became more pronounced for voltage amplitudes above 200 kV and for RT—reflector gap smaller than 30 mm. To avoid this plasma formation and the resulting parasitic electron flows and increasing the reflector transparency, improvement in the design of the reflector will be required.

V. DISCUSSION AND SUMMARY

The experiment presented in Sec. IV did not reproduce the electron bunching predicted by the simulations in Sec. II. This is not completely surprising as the simulations reproduced only partially the experimental conditions. The experiment has been successful in producing a periodic train of ∼40 A, 2 ns long electron bunches at a frequency of ∼200 MHz independent of the geometrical parameters which were varied. No current oscillations appear in the absence of the reflector.

By comparing Figs. 1–7, one can see some differences between the experimental setup and the model. The simulations in Sec. II did not model the upstream RTs and the large upstream cavity connecting the system to the generator. We have seen in Sec. II that the eigenfrequency of the downstream cavity is 1.35–0.89 GHz for $d_C = 11$–14 cm, respectively. The calculated eigenfrequency of the upstream cavity is 369 MHz. The eigenfrequencies of these two cavities differ greatly in value and the coupling between these two cavities can be considered to be weak because only a narrow channel connects them. Thus, the interaction of an electron flow with each of the cavities can be considered separately, and the mutual influence, if any, is small. This assumption is confirmed by numerical simulations in which the two upstream RTs and the large upstream cavity connecting the system to the generator are included and the reflector geometrical transparency is only of 50% (Fig. 10). Instead of a fixed axial magnetic field, we used the magnetic field measured along the axis of the experimental system

and applied these values over the entire calculation volume. A voltage pulse of 150 kV rising in 20 ns is applied on the left boundary of this system, and the emitter is assumed to be a single longitudinal mesh cell at the edge of the annular cathode. Electron emission starts at ∼8.5 ns when a predefined electric field threshold is reached during the voltage rise time. A slice of this volume and the simulated positions of the electrons at 140 ns is shown in Fig. 10(a). One can see that some current arrives at the collector and some to the walls of the upstream cavity. Negligible currents are collected on the anode or the central rod. In Fig. 10(b), we draw the currents collected on the Faraday cup and the walls of the upstream cavity.

The current collected on the Faraday cup in Fig. 10(b) appears with a delay of 9.5 ns from the onset of the applied voltage. It rises first fast, then drops, and then it rises again to a level of ∼10 A. The analysis of the electron axial momentum phase space distribution shows that it takes ∼17 ns (relative to the beginning of the electron emission) for electrons to reach the upstream walls when the current collected there levels at ∼5 A. The first peak in the collector current is related to electrons penetrating the reflector prior to the return current from the reflected electrons reaching the emitter, thus decreasing electron emission. Most of the charge is contained and circulated in the squeezed state formed between the upstream RT and the reflector. The spectrum of the current collected on the Faraday cup [Fig. 10(b)] is presented in Fig. 10(c). There is a peak in the spectrum at ∼1.1 GHz, close to the eigenfrequency of the downstream cavity, and two smaller peaks at 350 and 373 MHz, close to the eigenfrequency of the upstream cavity (369 MHz). These oscillations are of much smaller amplitudes than those observed in the experiment. Thus, the incorporation of the downstream cavity in the simulation domain, the correction of the magnetic field configuration, and the reflector transparency in accordance with the experimental conditions reduce the difference between the results of experiment and numerical simulations, namely, a low frequency component appears in the calculated spectrum and the amplitude of the high frequency component is not so high. Nevertheless, substantial discrepancies between experimental and numerical results remain.

There are two possible reasons for these discrepancies. First, the experimental emitter is significantly different from that simulated because it produces a radially expanding plasma from which electrons are emitted in both axial directions. Second, the simulations do not reproduce parasitic emission of electrons from the reflector and its ring-type holder, as well as ion flow from the plasma formed at the surface of the anode downstream flange. The latter can completely or partially neutralize space charge of electron bunches in the downstream cavity, decreasing the coupling with the cavity eigenmode. In the next experiments, we are planning to change the design of the cathode and the reflector holder to prevent backward parasitic current from the emitter and the holder.

ACKNOWLEDGMENTS

The authors are grateful to S. Gleizer and E. Flyat for their invaluable technical assistance.

DATA AVAILABILITY

The data that support the findings of this study are available from the corresponding author upon reasonable request.

REFERENCES

[1]B. N. Brejzman and D. D. Ryutov, Nucl. Fusion **14**, 873 (1974).
[2]L. S. Bogdankevitch and A. A. Rukhadze, Sov. Phys. Usp. **14**, 163 (1971).
[3]A. M. Ignatov and V. P. Tarakanov, Phys. Plasmas **1**, 741 (1994).
[4]S. Y. Belomyttsev, A. A. Grishkov, S. D. Korovin, and V. V. Ryzhov, Tech. Phys. Lett. **29**, 666 (2003).
[5]A. A. Grishkov, S. Y. Belomyttsev, S. D. Korovin, and V. V. Ryzhov, Tech. Phys. Lett. **29**, 944 (2003).
[6]S. Y. Belomyttsev, A. A. Grishkov, S. A. Kitsanov, S. D. Korovin, S. D. Polevin, V. V. Ryzhov, and A. P. Yachnyi, Tech. Phys. Lett. **31**, 982 (2005).
[7]J. G. Leopold, Y. P. Bliokh, M. Siman-Tov, and Y. E. Krasik, Phys. Plasmas **26**, 093107 (2019).
[8]A. E. Dubinov, A. G. Petrik, S. A. Kurkin, N. S. Frolov, A. E. Koronovskii, and A. E. Hramov, Phys. Plasmas **24**, 073102 (2017).
[9]M. I. Fuks, S. Prasad, and E. Schamiloglu, IEEE Trans. Plasma Sci. **44**, 1298 (2016).
[10]J. A. Karakkad, G. S. Nusinovich, B. L. Beaudoin, A. C. Ting, A. H. Narayan, and T. M. Antonsen, Jr., Phys. Plasmas **26**, 093101 (2019).
[11]T. J. Kwan, M. A. Mostrom, and B. B. Godfrey, Phys. Rev. Lett **66**, 3221 (1991).
[12]K. G. Kostov and J. J. Barroso, Int. J. Infrared Milimeter Waves **19**, 1513 (1998).
[13]J. J. Barroso, IEEE Trans. Plasma Sci. **28**, 652 (2000).
[14]B. Goplen, L. Ludeking, D. Smith, and D. Warren, Comput. Phys. Commun. **87**, 54 (1995).
[15]Y. E. Krasik, A. Dunaevsky, A. Krokhmal, J. Felsteiner, A. V. Gunin, I. V. Pegel, and S. D. Korovin, J. Appl. Phys. **89**, 2379 (2001).
[16]J. Z. Gleizer, T. Queller, Y. Bliokh, S. Yatom, V. Vekselman, Y. E. Krasik, and V. Bernshtam, J. Appl. Phys. **112**, 023303 (2012).
[17]T. Queller, A. Shlapakovski, and Y. E. Krasik, J. Appl. Phys. **108**, 103302 (2010).
[18]*Pulse Power Formulary*, edited by R. J. Adler (North Star Research Corporation, 2002).
[19]S. P. Bugaev, V. I. Kanavez, V. I. Koshelev, and V. A. Cherepanov, *Relativisitic MulitiWave Microwave Generators* (Sibirian Division, Novosibirsk, Nauka, 1991) (in Russian).
[20]S. Y. Belomyttsev, V. V. Rostov, I. V. Romanchenko, S. A. Shunailov, M. D. Kolomiets, G. A. Mesyats, K. A. Sharypov, V. G. Shpak, M. R. Ulmaskulov, and M. I. Yalandin, J. Appl. Phys. **119**, 023304 (2016).
[21]S. P. Bougaev, A. A. Kim, A. I. Klimov, and V. I. Koshelev, "Study of cathode plasma expansion in high current magnetically insulated diodes," in the Proceedings of the 4th International Topical Conference on High-Power Electron and Ion Beam Research & Technology, Palaiseau, France (1981), pp. 401–408.